Transport of C-13-oleate in adipocytes measured using multi imaging mass Spectrometry

ARTICLE *in* JOURNAL OF THE AMERICAN SOCIETY FOR MASS SPECTROMETRY · DECEMBER 2004

Impact Factor: 2.95 · DOI: 10.1016/j.jasms.2004.07.010 · Source: PubMed

3 AUTHORS, INCLUDING:

Claude Lechene
Brigham and Women's Hospital
138 PUBLICATIONS **4,558** CITATIONS

Transport of ^{13}C-Oleate in Adipocytes Measured Using Multi Imaging Mass Spectrometry

Alan M. Kleinfeld and J. Patrick Kampf
Torrey Pines Institute for Molecular Studies, San Diego, California, USA

Claude Lechene
Harvard Medical School and Brigham and Women's Hospital, Cambridge, Massachusetts, USA

The mechanism of long chain free fatty acid (FFA) transport across cell membranes is under active investigation. Here we describe the use of multi imaging mass spectrometry (MIMS) to monitor intracellular concentrations of FFA and provide new insight into FFA transport in cultured adipocytes. Cells were incubated with ^{13}C-oleate:BSA and either dried directly or dried after washing with a medium deprived of ^{13}C-oleate:BSA. Cells were analyzed with MIMS using a scanning primary Cs^+ ion beam and $^{12}C^-$, $^{13}C^-$, $^{12}C^{14}N^-$, $^{13}C^{14}N^-$ (or $^{12}C^{15}N^-$) were imaged simultaneously. From these quantitative images the values of the $^{13}C/^{12}C$ ratios were determined in the intracellular lipid droplets, in the cytoplasm and outside the 3T3F442A adipocytes. The results indicate that after incubation with ^{13}C-oleate:BSA the droplet $^{13}C/^{12}C$ ratio was 15 ± 6%. This value is about 14-fold higher than the $^{13}C/^{12}C$ terrestrial ratio (1.12%). After washing the ^{13}C-oleate:BSA, the droplet $^{13}C/^{12}C$ ratios decreased to 1.6 ± 0.1%, about 40% greater than the natural abundance. Results for washed cells indicate that relatively little FFA was esterified. The unwashed cell results, together with the value of the lipid water partition coefficient, reveal that intracellular unbound FFA (FFA_u) concentrations were on average about 4.5-fold greater than the extracellular FFA_u concentrations. These results are consistent with the possibility that FFA may be pumped into adipocytes against their electro-chemical potential. This work demonstrates that MIMS can be used to image and quantitate stable isotope labeled fatty acid in intracellular lipid droplets. (J Am Soc Mass Spectrom 2004, 15, 1572–1580) © 2004 American Society for Mass Spectrometry

In this report we describe a novel approach to study cellular transport of free fatty acids (FFA) that uses the combination of corrective ion optics with secondary ion mass to quantitatively image the intracellular distribution of stable-isotope (^{13}C) labeled FFA in 3T3F442A adipocytes.

Despite the importance of FFA for life, studies of FFA transport are difficult to extend to the cellular scale due to the lack of suitable methodology. Autoradiography of radioactive labels cannot provide quantitative information on FFA accumulation in intracellular fat droplets, while fluorescently labeled FFA may not accurately reflect the transport and metabolism of native FFA.

Although imaging of biological tissues has been provided by secondary ion mass spectrometry [1–12], quantitation of isotope ratios in secondary ion mass spectrometry of biological tissue has been problematic.

A new type of secondary ion mass spectrometer, equipped with the dual capabilities of simultaneously measuring several ion masses and imaging at high resolution, has recently been developed [13]. With this multi-isotope imaging mass spectrometer (MIMS [the MIMS instrument used in these studies is the prototype of the NanoSims50, Cameca, France]), the intensity currents for several secondary ions can be obtained simultaneously, so that determination of isotope ratios is independent of changes in instrumental or sample conditions. We have previously used MIMS to directly measure $^{13}C/^{12}C$ and $^{15}N/^{14}N$ isotope ratios in cultured cells at a subcellular scale [14] and used these results to demonstrate a high rate of protein turnover in cochlear stereocilia interconnecting links [15]. Here we report the use of MIMS to study the accumulation of ^{13}C labeled oleic acid in intracellular lipid droplets of cultured adipocytes.

FFA are critical for many physiological processes. Fatty acids are transported in the blood bound to albumins and they cross the plasma membrane to be stored as triacylglycerol in the lipid droplets of adipocytes. FFA transport across the plasma membrane is central to the principal function of the adipocyte, the

Published online September 18, 2004

Address reprint requests to Alan Kleinfeld, Torrey Pines Institute for Molecular Studies, 3550 General Atomics Court, San Diego, CA 92121, USA.
E-mail: akleinfeld@tpims.org

1044-0305/04/$30.00
doi:10.1016/j.jasms.2004.07.010

Received May 17, 2004
Revised July 14, 2004
Accepted July 14, 2004

storage and release of FFA from intracellular triacylglycerol. The nature of the transport mechanism of FFA from the aqueous phase on one side to the aqueous phase on the other side of cell membranes remains uncertain (for recent reviews see: [16–21]). In one view, transport of FFA across cell membranes is thought to require membrane proteins [22–25]. In a second view, transport of FFA is reported to undergo rapid flip-flop through the lipid bilayer phase, thereby obviating the need for a protein- mediated process [26–30]. Much of the uncertainty has its basis in the methodological difficulties of monitoring FFA [31, 32].

Using quantitative imaging with MIMS we have directly studied the accumulation of ^{13}C in cultured adipocytes incubated with ^{13}C labeled oleic acid. We measured a high level of ^{13}C accumulation in intra cellular lipid droplets. This result is best explained by a protein-mediated process for FFA transport.

This study indicates that MIMS provides a new and important approach for studying cellular transport and metabolism of FFA. Using MIMS, movement of native FFA can be traced to specific subcellular locations and accurate isotope ratios allow the concentration of FFA to be determined at subcellular sites. The results of this study provide the first images and relative concentration measurements of FFA in the lipid droplets of adipocytes. The results are consistent with the possibility that FFA may be pumped into adipocytes against their electro-chemical potential.

Methods

MIMS Analysis

The samples were analyzed with multi-isotope quantitative imaging mass spectrometry, using the prototype of a new generation of secondary ion mass spectrometer [13, 33] (factory prototype of the NanoSims50, Cameca, Courbevoie, France). The primary beam directed at the sample was Cs^+ accelerated at 16 kV. The vacuum in the analysis chamber was around 3×10^{-10} torr. We analyzed in parallel the secondary ions $^{12}C^-$, $^{13}C^-$, $^{12}C^{14}N^-$, $^{13}C^{14}N$ (or $^{12}C^{15}N^-$) emitted from the samples.

Secondary-Ion Counting

Each species of secondary ion was detected with an electron multiplier. The high voltage applied to each electron multiplier and the pulse-height discriminator on its output were adjusted together to maintain the highest efficiency of detecting secondary-ion impacts while discarding noise and having an equivalent counting efficiency among the four counters.

Tuning for Mass Selection

The first level of mass selection for discriminating the secondary ions was provided by individual trolleys, each with an electron multiplier, that were moved to the desired radii of curvature for the masses of interest (based on the kinetic energy of the secondary ions and the magnetic field strength of the mass spectrometer). One trolley was positioned for detecting mass 12, a second one for mass 13, a third one for mass 26, and a fourth one for mass 27.

High mass resolution was obtained by adjusting deflection plates positioned just before each electron multiplier as described in [14]. This procedure allows for mass resolutions that discriminate between isobars such as $^{13}C^-$ (mass 13.003355) and $^{12}C^1H^-$ (mass 13.007825), $^{12}C^{14}N^-$ (mass 26.003074) and $[^{13}C]_2^-$ (mass 26.00671), and $^{12}C^{15}N^-$ (mass 27.000109), $^{13}C^{14}N^-$ (mass 27.006429) and $^{12}C^{14}N^1H^-$ (mass 27.010899). By appropriately setting the deflection-plate voltages of the detectors, one can determine for each detector which isobar is detected by the electron multiplier, eliminating any spill-over from neighboring mass peaks.

Simultaneous Quantitative Secondary-Ion Images

Images of cells were produced by scanning a highly focused primary ion beam (35–50 nm) stepwise in one raster across the sample. The adaptive ion optics correct for aberrations and match the shape of the secondary ion beam to the acceptance of the mass spectrometer and detectors, maintaining high transmission of secondary ions. Dynamic transfer insured that while the primary ion beam step scanned the sample, the secondary ion beam position was compensated so as to be stationary, and thus entered the detector in a fixed position. Four detectors recorded the secondary ions of selected masses produced simultaneously from a given sample region. Thus, mass density distribution images of the selected species were in exact registration with each other. Simultaneous images of the distributions of ^{12}C, ^{13}C, $^{12}C^{14}N^-$, $^{13}C^{14}N^-$, or $^{12}C^{15}N^-$ emitted as secondary ions from the surface of a sample were obtained. The beam current and diameter, dwell time per pixel, and step size were adjusted according to the size of the area being analyzed; a step raster of 256 by 256 pixels was generally used. In the scanning mode, the number of counts for each secondary ion emitted from each pixel was stored as a 16-bit integer in a computer file. Grayscale secondary-ion images for each of the selected secondary ions were obtained after analysis by reconstructing the data onto a 256 by 256 pixel array, with the pixel intensity in the image scaled according to the number of counts detected from that position.

Hue Saturation Intensity (HSI) Transform

Images acquired with MIMS have a dynamic range of 16 bits and resulting ratios generate far more information than can be easily displayed using simple gray level methods. In order to identify those pixels with significantly different isotope ratios than their neighbors we use a hue saturation intensity transformation of

the ratio image [15]. The resulting image displays the ratios in rainbow colors with a hue corresponding to a given ratio value and the intensity of the hue coding for the significance of the values.

Quantitative Ratios

Regions of interest (ROIs) were selected from the HSI $^{13}C/^{12}C$ image and the same ROIs were selected from the corresponding image of $^{12}C^-$, $^{13}C^-$, $^{12}C^{14}N^-$, and $^{13}C^{14}N^-$. The isotope ratio for each region of interest was determined by dividing the total counts of $^{13}C^-$ over all pixels in that region by the total corresponding counts of $^{12}C^-$and dividing the total counts of $^{13}C^{14}N^-$ (or $^{12}C^{15}N^-$) over all pixels in that region by the total corresponding counts of $^{12}C^{14}N^-$. The precision of these ratios was essentially determined by the number of counts for $^{13}C^-$, $^{13}C^{14}N^-$, and $^{12}C^{15}N^-$, respectively, which was generally larger than 1000 (3% precision) even in the smallest regions of interest. Data analysis was performed with an SGI O2 workstation using Isee Analytical Imaging Software (Inovision Corporation, Raleigh, NC) and special software developed with NSee Corporation (Raleigh, NC).

Adipocyte Preparation

3T3-F442A adipocytes [34] cultured in 25 cm^2 flasks were trypsinized and washed with phosphate buffered saline. Approximate cell density was determined by counting with a hemocytometer. Ten percent FCS in DMEM with 10 μg/mL insulin was added to 6×10^5 cells/mL in a 1.3:1 ratio. The cells were then added to a petri dish containing ten 0.5 cm^2 silicon chips and placed in an incubator at 37 °C, 5% CO_2, and 95% relative humidity to allow the cells to adhere to the silicon surface. After 3 h, the medium was exchanged for fresh 10% FCS in DMEM with 10 μg/ mL insulin. The cells were then allowed to incubate overnight. One silicon chip was used for examination with a light microscope to ascertain the presence of adherent adipocytes.

Transport Procedure

The remaining silicon chips with adherent adipocytes were divided between three wells of a 24- well plate. Each well was washed twice with C-HEPES. Then 300 μL of 6:1 ^{13}C-oleate:BSA was added to each well, and the plate was placed in an incubator at 37 °C for 20 min. From this point forward the cells were treated in three different ways: (1) not washed, (2) washed with C-HEPES, and (3) incubated in 600 μM BSA. In the first treatment, the silicon chips were removed from the 24-well plate and dried immediately with argon. In the second procedure, the cells were washed with C-HEPES and then dried with argon. In the last case, the ^{13}C-oleate:BSA was removed from the well and 600 μM BSA was added after which the cells were allowed to incubate for 10 min. Again the silicon chips were removed and dried. Dried cells were stored at −4 °C prior to the MIMS experiment. In all cases the ^{13}C-oleate:BSA was recovered from each well and measured again with ADIFAB [35] to verify that the free concentration of ^{13}C-oleate did not change after exposure to the cells.

Preparation of ^{13}C-OA and Complexes with BSA

Prior to preparation of the oleate:BSA complex, ^{13}C-oleic acid was saponified with sodium hydroxide. Concentrated sodium hydroxide solution (50% wt/wt) was added in 75% excess to 0.2 M ^{13}C-OA in methanol. The resultant sodium salt was dried under argon and placed in an argon- filled dessicator for 1 h to remove excess methanol and water. A 24 mM stock solution of sodium ^{13}C-oleate was prepared by dissolving the dried solid in de-ionized water at 37 °C. The ^{13}C-oleate stock solution was stored in the dark at −20 °C prior to use.

The primary buffer used for the transport study consisted of 20 mM HEPES, 140 mM NaCl, 5.5 mM glucose, 5 mM KCl, 1 mM NaH_2PO_4, 1 mM $CaCl_2$, and 1 mM $MgSO_4$ in deionized water at pH 7.4 (C-HEPES). Approximately 600 μM stock solutions of BSA were made in C-HEPES for preparation of oleate:BSA complexes. An approximately 6:1 complex of ^{13}C-oleate bound to BSA was prepared by adding, while mixing, small aliquots (< 30 μL) of the 24 mM ^{13}C-oleate stock solution to a solution of 600 μM BSA at 37 °C. One aliquot was added every 2 min, and the final aqueous free concentration was determined to be of 250 nM ^{13}C-oleate by direct measurement with ADIFAB at 37 °C. The oleate:BSA complex and BSA stock were stored at −20 °C prior to transport experiments.

Estimation of the Intracellular Aqueous Concentration of FFA ([FFA$_i$])

[FFA$_i$] can be estimated from the $^{13}C/^{12}C$ ratios in the intracellular lipid droplets under the assumption that the concentration of FFA within the lipid droplet is in equilibrium with [FFA$_i$]. This equilibrium is characterized by a partition coefficient (K_p) determined for lipid vesicles [36] and confirmed for dispersions of triacylglycerol (TAG) (unpublished results). It follows that the concentration of FFA within the droplet phase ([FFA$_d$]) is = K_p*[FFA$_i$] and the concentration of FFA$_d$ carbons for oleate is 18*[FFA$_d$]. The concentration of carbons within the lipid droplet, assuming the droplet is composed entirely of TAG (Mw ~ 885) and has a specific density of 0.9, is 56 M (about 55 carbons/ TAG and [TAG] = 1.02M). Thus the mole fraction of FFA carbons to total droplet carbons is about 18* K_p*[FFA$_i$]/56. In this report the unbound extracellular oleate was 250 nM. If [FFA$_i$] were also 250 nM then for oleate with all 18 carbons labeled with ^{13}C, the ^{13}C concentration within the lipid droplet due to oleate would be 1.75 M ($K_p = 4 \times 10^5$). Therefore, if [FFA$_i$] = [FFA$_o$] the total

Table 1. Secondary ion yield (counts/sec)

	1-^{13}C OA 25 mM		$^{13}C_{18}$ OA 24 mM		$^{13}C_{18}$ OA (3.9 mM) + BSA (0.6 mM)	
Statistic	^{12}C	^{13}C	^{12}C	^{13}C	^{12}C	^{13}C
Mean	112733	5372	2534	63726	13898	597
S.D.	14620	782	816	18955	2651	129
C.V.	0.13	0.15	0.32	0.3	0.19	0.22

^{13}C/^{12}C ratio (natural abundance of 1.1% plus the ^{13}C-oleate) within the droplet should be 1.1 + 3.1 = 4.2%.

"Drop" Control Experiments

In initial experiments we compared the yield of secondary ions from oleic acid, either labeled at the carbon of the carboxy group (oleic-1-^{13}C-acid) or labeled at all carbons (oleic-$^{13}C_{18}$-acid): 25 mM 1-^{13}C oleic acid, 24 mM $^{13}C_{18}$ oleic acid and 3.9 mM $^{13}C_{18}$ oleic acid with 0.6 mM BSA in HEPES buffer. Each OA sample was saponified as described and the salt was dissolved in water at concentrations of 25 and 24 mM, respectively. Samples were spotted on Si wafers as 1 μl drops and dried under argon. After evaporation of the solvent a central drop formed surrounded by a ring of material thin enough to show interference colors. To investigate whether a fractionation of the components had occurred during the evaporation process, readings were taken along a radius at five positions of different interference colors from the most peripheral to the innermost ring and in the central drop.

Materials

Oleic acid with ^{13}C at all 18 carbon positions (^{13}C-OA) was purchased from Isotec, Inc. (Miamisburg, OH). ADIFAB was prepared as described previously [35] and can be purchased from FFA Sciences, LLC (San Diego, CA). HEPES was purchased from ICN Biomedicals, Inc. (Aurora, OH). Essentially fatty acid free BSA, trypsin, insulin, and remaining buffer components were obtained from Sigma-Aldrich (St. Louis, MO). DMEM was purchased from Gibco BRL (Gaithersburg, MD) and phosphate buffered saline was purchased from BioWhittaker (Walkersville, MD). Fetal calf serum (FCS) was obtained from Tissue Culture Biologicals (Tulare, CA). 3T3-F442A adipocytes were converted from preadipocyte fibroblasts as described [34]. Silicon wafers were purchased through Montco Silicon Technologies, Inc. (Spring City, PA). They have resistivity between 0.005–0.020 ohm cm and a thickness between 475–575 microns. The wafers were cut into 0.5 cm squares at MIT in the Microsystems Technology Laboratories (Cambridge, MA).

Results

"Drop" Control Experiments

The secondary ion yield and the isotope ratios for the three types of samples are shown in Tables 1 and 2, respectively. The isotope ratios were equivalent among the different positions of analysis.

Transport Experiments

MIMS was used to monitor ^{13}C-oleate transport in 3T3F442A adipocytes by monitoring ^{13}C/^{12}C ratios. Monolayers of cells were grown on silicon chips and, after treatment to alter the concentration of extracellular ^{13}C-oleate, the cells were dried with argon. We used three experimental protocols designed to alter the amount of FFA that may accumulate in the intracellular lipid droplets. In one protocol cells were incubated at 37 °C for 20 min with the ^{13}C-oleate:BSA complex in which [^{13}C-oleate] was 3.6 mM and [BSA] was 600 μM and the incubation was halted by drying the cells with argon. In a second protocol, cells were treated as above but then washed for 10 min by incubation with fatty acid free BSA, which was removed before drying. In a third one, cells were treated with the ^{13}C-oleate:BSA complex and then washed with C-HEPES.

Quantitative MIMS images were obtained in parallel for $^{12}C^-$, $^{13}C^-$, $^{12}C^{14}N^-$, and the isobars, $^{13}C^{14}N^-$ or $^{12}C^{15}N^-$. The region of interest was evaluated at three different locations: Outside the cell, inside the cell (outside the lipid droplets) and in the lipid droplets.

Imaging. The mass images of an adipocyte that had been exposed to ^{13}C oleic acid for 20 min are shown in Figure 1. The mass images of the $^{12}C^-$ and $^{12}C^{14}N^-$ ions (Figure 1a, d) detail the cell histology. Note that the contrast revealed in these images was obtained in the absence of any stain or enhancing agent. The mass

Table 2. Isotope ratios [^{13}C/(^{12}C + ^{13}C)]

Statistic	1-^{13}C OA 25 mM	$^{13}C_{18}$ OA 24 mM	$^{13}C_{18}$ OA (3.9 mM) + BSA (0.6 mM)
Mean	0.045	0.962	0.041
S.D.	0.002	0.003	0.002
C.V.	0.045	0.003	0.061

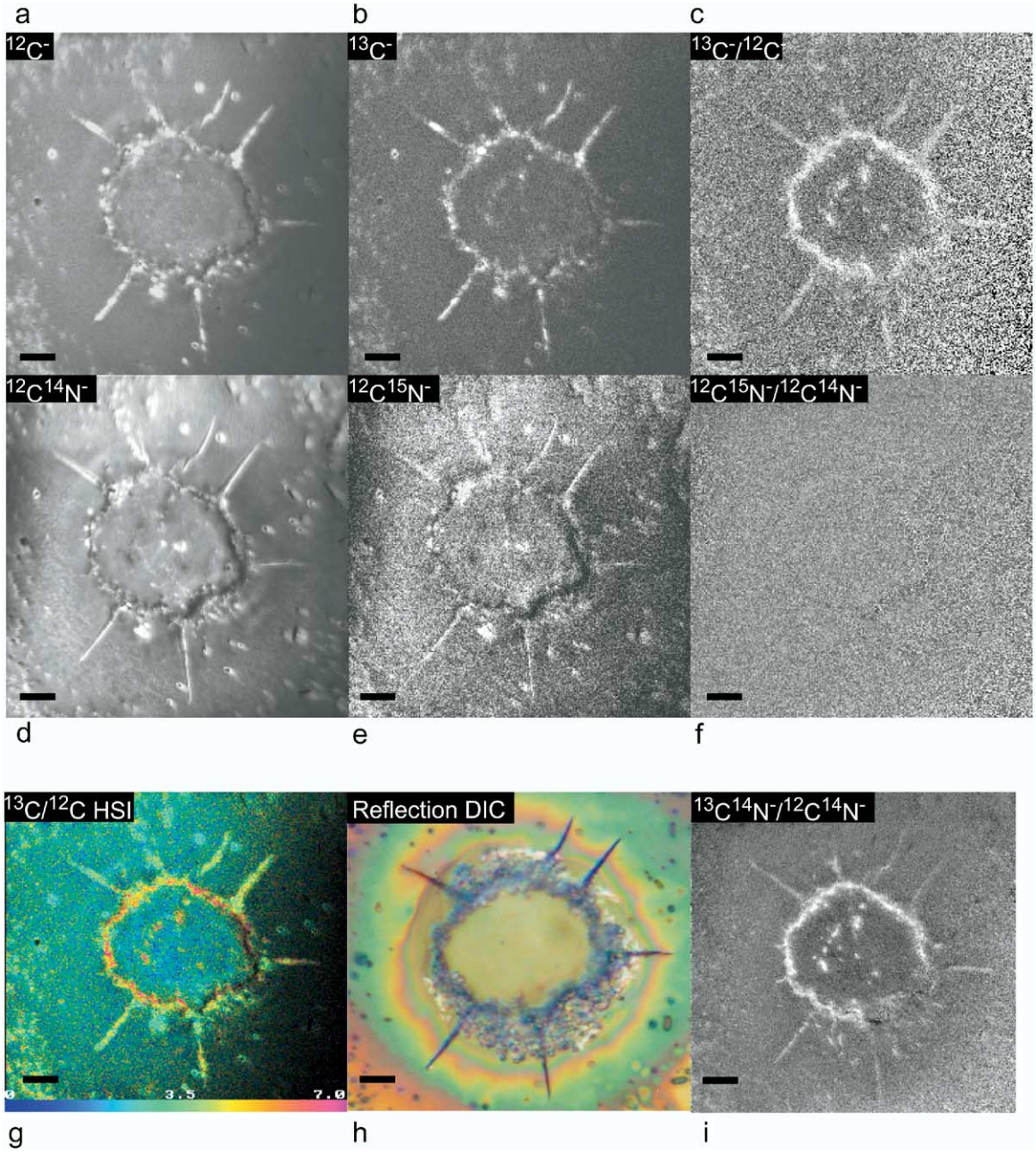

Figure 1. Unwashed 3T3F442A cells treated with ^{13}C-oleate:BSA. Images of cells dried with argon after incubation with ^{13}C-oleate. (**a**)–(**e**) are MIMS mass images of $^{12}C^-$ (**a**), $^{13}C^-$ (**b**), $^{12}C^{14}N^-$ (**d**), and $^{12}C^{15}N^-$ (**e**), and their respective ratio images of $^{13}C/^{12}C$ (**c**) and $^{12}C^{15}N^-/^{12}C^{14}N^-$ (**f**). A hue saturation intensity (HSI) image of the $^{13}C/^{12}C$ ratios is shown in (**g**); (**h**) is a reflection differential interference contrast (DIC) image of the same cells before analysis with MIMS. In addition (**i**) is the $^{13}C^{14}N/^{12}C^{14}N$ distribution that reveals the excess ^{13}C in the lipid; (**g**–**i**) reveal the peripheral distribution of lipid droplets. DIC images (500×) were obtained using a Nikon Eclipse E800 upright microscope. The MIMS images are 60 μm × 60 μm, 256 × 256 pixels and were acquired in 40 min. The total counts for the mass images are: (**a**) 2.11×10^7, (**b**) 6.60×10^5, (**d**) 1.30×10^8, (**e**) 3.92×10^5. Total counts from the images used to generate (**i**) are 1.21×10^7 for $^{13}C^{14}N$ and 5.08×10^8 for $^{12}C^{14}N$. The scale bar in all panels is 5μm in length.

image of the $^{13}C^-$ ions (Figure 1b) is similar to the $^{12}C^-$ ions mass image in form but has a lower count rate. The pixel counts of the $^{13}C^-$ ions image reflect the adipocyte voxel content of both the natural ^{13}C and the supplement of ^{13}C coming from the ^{13}C oleic acid transported inside the cell. This supplement of ^{13}C is at a maximum at the intracellular lipid droplets, where FFA accumulates. The mass image of the $^{12}C^{15}N^-$ ions (Figure 1e) is similar to the $^{12}C^{14}N^-$ ions mass image (Figure 1d), yet with a much lower count rate. Each voxel of the sample

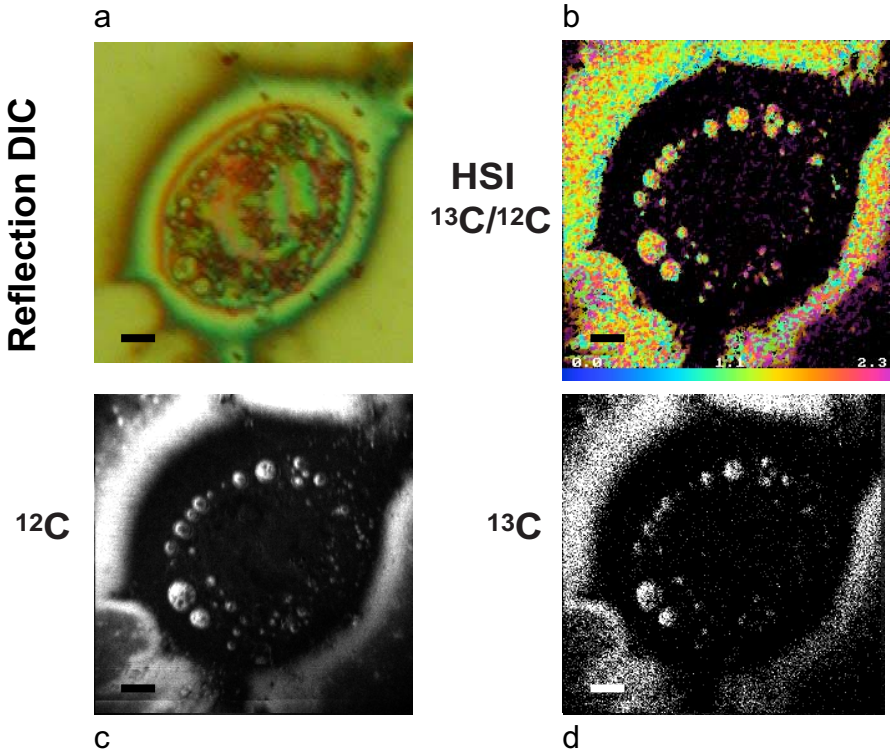

Figure 2. 3T3F442A cells treated with ^{13}C-oleate:BSA and buffer washed. Light microscopy (DIC) and MIMS images of cells after incubation with ^{13}C-oleate, washing with buffer and drying under argon. Both imaging methods reveal the peripheral distribution of discrete lipid droplets that is typical of these cells. ^{13}C and ^{12}C images were used to image ^{13}C/ ^{12}C, here represented as a hue saturated image with a range from 0 to 2.3, and to determine the ^{13}C/^{12}C values at different regions of interest both outside and inside the cells. DIC images (500×) were obtained using a Nikon Eclipse E800 upright microscope. The MIMS images are 60 μm × 60 μm, 256 × 256 pixels and were acquired in 30 min. Total counts in the ^{12}C and ^{13}C images are 5.75×10^6 and 8.25×10^4, respectively. The scale bar in all panels is 5 μm in length.

resulting in the $^{12}C^{15}N^-$ ions image contains the fraction of ^{15}N related to the ^{14}N content by the natural ratio of $^{15}N/^{14}N$.

The ratio images of $^{13}C^-/^{12}C^-$ and $^{12}C^{15}N^-/^{12}C^{14}N^-$ (Figure 1c, f) result from the pixel-by-pixel division of the $^{13}C^-$ image by the $^{12}C^-$ image and of the $^{12}C^{15}N^-$ image by the $^{12}C^{14}N^-$ image, respectively. The enhanced contrast observed in the $^{13}C^-/^{12}C^-$ image is due to the excess ^{13}C incorporated in the lipid droplets from the ^{13}C oleic acid transported from the outside medium. The $^{12}C^{15}N^-/^{12}C^{14}N^-$ image has no contrast because in the absence of exogeneously added ^{15}N, the value of the ratio of $^{15}N/^{14}N$ is equivalent to the natural ratio across the analyzed field.

In Figure 1g is the HSI image of $^{13}C/^{12}C$ ratios and panel h is the same cell photographed by reflection differential interference contrast microscopy on the silicon chip, before analysis by MIMS. Figure 1i is the $^{13}C/^{12}C$ ratio measured as the cyanide ion, $^{13}C^{12}N^-/^{12}C^{14}N^-$, and also shows accumulation of ^{13}C in the droplets.

Quantitation. Cells that were incubated with ^{13}C-oleate:BSA, but not washed, had very high $^{13}C/^{12}C$ ratios in the lipid droplets (Figures 1c, g). Values (average and standard deviation) for $^{13}C/^{12}C$ in the three regions were 2.5 ± 0.5%, 1.9 ± 0.2% and 15 ± 6%, for inside, outside and droplet regions, respectively. In particular the lipid droplet $^{13}C/^{12}C$ for the unwashed cells is 14-fold greater than the natural abundance and is 4.5-fold greater than the amount expected (3.1%) for equal inside and outside FFA_u levels.

In contrast to the high values of $^{13}C/^{12}C$, buffer and BSA (data not shown) washed cells had low $^{13}C/^{12}C$ ratios (Figure 2a-d). Both yielded values for $^{13}C/^{12}C$ ratios that were only slightly higher than the natural abundance of ^{13}C (1.1%). However, the ratios in the three locations revealed a distinct pattern with lowest values in non- droplet regions inside the cells (1.3 ± 0.1%), intermediate values outside (1.5 ± 0.1%) and the highest values within the lipid droplets (1.6 ± 0.1%).

In cells not treated with ^{13}C-OA, the value of the $^{13}C/^{12}C$ ratio measured under the same conditions was 1.15 ± 0.10, not significantly different from the terrestrial $^{13}C/^{12}C$ value of 1.12. Also, an indication of the accuracy of these ratio values was obtained from measurements of the $^{12}C^{15}N/^{12}C^{14}N$ ratios, whose value was 0.36 ± 0.01% in both washed and unwashed cells

and is in excellent agreement with the natural abundance of 0.37%.

Discussion

MIMS is a new quantitative imaging method capable of quantitation of isotopic molecular tags coincident with acquisition of an ultrastructural image. As such it is an immense step forward from the use of radioactive isotopes in "autoradiography" and it will open many new avenues for research in biology and biomedical sciences. MIMS can be used with animal tissue or with isolated cells from a tissue culture preparation using conventional methods for preparing sample for ultrastructural analysis. We illustrate the power of the new machine using the stable ^{13}C isotope of carbon in a study of fatty acid accumulation in adipocyte lipid droplets, which would be impossible with autoradiography of ^{14}C because of poor resolution and lack of precise quantitation.

Determining intracellular isotope ratios of carbon requires measuring the count rates of two secondary ions in parallel from the same sample volume under the same conditions. Single channel SIMS has been limited to the evaluation of one secondary ion count rate at a time, thus introducing potential sources of errors in the ratio determination due to the possibility of sample drift, sample degradation under the primary ion beam, or slight changes in instrumental conditions. On the other hand, current TOF-SIMS instruments have neither the spatial resolution for imaging droplets of about one micrometer diameter nor the mass resolution necessary to discriminate between isobars [6]. These difficulties, however, are resolved by MIMS, which permits the parallel detection of mass 12 simultaneously with mass 13, providing multiple secondary ion measurements from the same sputtered microscopic volume. The high mass resolving power of MIMS is illustrated by the isotope ratio quantitative image of the isobars $^{12}C^{15}N$ and $^{13}C^{14}N$, which are well separated ($M/\Delta M \approx 4300$) so that the $^{12}C^{15}N/^{12}C^{14}N$ ratio image is flat and equivalent to the terrestrial ratio (Figure 1f) while the $^{13}C^{14}N/^{12}C^{14}N$ ratio image (Figure 1i) shows accumulations of ^{13}C in the droplets.

The experiments in which solutions of oleate and oleate plus BSA were measured, show that fatty acids provide a good yield of secondary ions. The thickness of the layer has no significant effect on the yield (Table 1) and importantly no spatial fractionation was observed. The measured isotope ratios were equivalent among the varied position on the drops (Table 2). The measured isotope ratios are in good agreement with the predicted isotope ratios based on labeling and purity, although in all cases there is a dilution of the label (predicted for 1-^{13}C-OA: 6.57%, predicted for 18-^{13}C-OA: 99%). This most probably reflects isotope dilution due to contamination from extraneous carbon-containing compounds. The value of 4.3% of the $^{13}C/^{12}C$ ratio measured for the 3.9 mM $^{13}C_{18}$-OA plus 0.6 mM BSA is in good agreement with the value we calculated (4.7%) using the Swiss protein database to obtain the number (3071) of carbons/BSA.

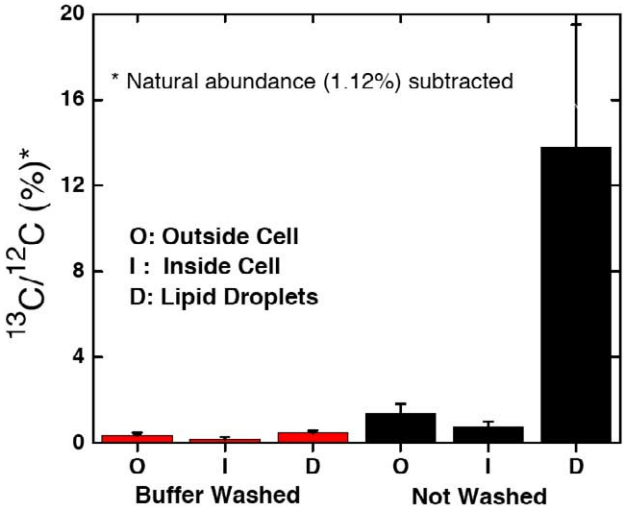

Figure 3. Excess $^{13}C/^{12}C$ values in regions of interest in 3T3F442A adipocytes. Values of $^{13}C/^{12}C$ were evaluated as averages and standard deviations of at least three regions of interest in locations outside the cells (O), inside but not in visible lipid droplets (I), and inside the lipid drop-lets (D). The results are the excess $^{13}C/^{12}C$ values after subtraction of the natural abundance of $^{13}C/^{12}C$ (1.12%).

Light microscopy (reflection differential interference contrast) and MIMS images yield similar cell morphologies, in particular they reveal the discrete intracellular lipid droplets that are characteristic of the 3T3F442A adipocytes (Figure 2).

The present MIMS results provide new information about the trafficking and metabolism of FFA in 3T3F442A adipocytes. Cells that were not washed revealed a more than 14-fold greater excess of ^{13}C (Figure 3). This value is 4.5-fold greater than the value expected if $[FFA_i] = [FFA_o]$.

Drying cannot be the cause of the large excess of ^{13}C in the lipid droplets. Indeed, such high $^{13}C/^{12}C$ ratios were not observed in non-droplet hydrophobic structures, for example intracellular membranes. Moreover, the quantity of free fatty acid estimated in the cytoplasm is much too small to provide the amount estimated in the lipid droplets. Also, the outside medium is quickly aspirated before drying and could not account for the quantity found in the droplets. Additionally, there is no segregation or formation of droplet-like clusters with high ratios of $^{13}C/^{12}C$ outside the adipocytes.

The relatively high $^{13}C/^{12}C$ ratio (2.5%) in regions outside unwashed cells is likely due to the presence of ^{13}C-oleate-BSA in the outside regions (the $^{13}C/^{12}C$ for ^{13}C-oleate-BSA itself is about 4.5%). The lower (1.9%) $^{13}C/^{12}C$ ratios in the inside, non-droplet regions, presumably reflect the presence of non-droplet hydrophobic, for example membrane, phases inside the cell.

The MIMS results are in agreement with direct

monitoring of FFA in the extracellular ([FFA_o]) and intracellular ([FFA_i]) aqueous phases using ADIFAB, a fluorescent monitor of the aqueous phase concentration of FFA [32]. This method uses fluorescence ratio microscopy of adipocytes microinjected with ADIFAB to image the temporal and spatial distribution of intracellular [FFA_u]. Using ADIFAB under the same conditions as for the present study, we found that [FFA_i] reaches steady state values within about 5 min and levels remain constant for times greater than 20 min in the presence of oleate:BSA complexes [32].

In contrast to the high excess ^{13}C levels found in the droplets of cells exposed to FFA without washing, the intracellular droplet levels of ^{13}C in the cells that were washed are only about 40% greater than natural abundance. This indicates that the unesterified FFA in the lipid droplets is rapidly extracted by washing and that less than 13% of the ^{13}C-oleate is esterified during the 20 min incubation with ^{13}C-oleate:BSA. This is consistent with the reduction of [FFA_i] to baseline levels within about 50 s that we found in ADIFAB measurements of adipocytes washed with fatty acid free BSA after exposure to oleate:BSA complex [32]. The small (0.4%) excess of ^{13}C remaining in the region outside the cell suggests incomplete washing.

MIMS results are consistent with the notion that FFA influx in 3T3F442A cells is up a concentration gradient [32]. In addition to the [FFA_i] value, the predicted level of excess ^{13}C in the lipid droplets depends on the value of the partition coefficient and on the assumption that FFA in the cytosol and in lipid droplets are at equilibrium. The rapid removal of [FFA_i] from the cytosol as determined by ADIFAB and from the lipid droplets as determined by MIMS provides support for rapid equilibrium between these two phases. Moreover, measurements of the FFA partition coefficients for different hydrophobic phases yield virtually identical results (for a particular molecular species of FFA) within experimental uncertainty [35, 37, 38].

In conclusion, MIMS can be used to investigate lipid metabolism with high spatial and quantitative resolution. Using MIMS we have shown, for the first time, that movement of native FFA can be traced to and measured at specific subcellular locations.

Acknowledgments

This work was supported in part from grants DK058762 from the National Institute of Diabetes and Digestive and Kidney Diseases and 9 P20 EB001974-04 from the National Center of Research Resources. The authors thank Molly Palmer for editorial assistance.

References

1. Hindie, E.; Hallegot, P.; Chabala, J. M.; Thorne, N. A.; Coulomb, B.; Levi-Setti, R.; Galle, P. Ion Microscopy: A New Approach for Subcellular Localization of Labeled Molecules. *Scanning Microsc.* **1988,** *2*(4), 1821–1829.
2. Burns, M. S. Biological Microanalysis by Secondary Ion Mass Spectrometry: Status and Prospects. *Ultramicroscopy* **1988,** *24*(2/3), 269–281.
3. Hindie, E.; Coulomb, B.; Beaupain, R.; Galle, P. Mapping the Cellular Distribution of Labeled Molecules by SIMS Microscopy. *Biol. Cell* **1992,** *74*(1), 81–88.
4. Hindie, E.; Coulomb, B.; Galle, P. SIMS Microscopy: A Tool to Measure the Intracellular Concentration of Carbon 14-Labeled Molecules. *Biol. Cell* **1992,** *74*(1), 89–92.
5. Clerc, J.; Fourre, C.; Fragu, P. SIMS Microscopy: Methodology, Problems, and Perspectives in Mapping Drugs and Nuclear Medicine Compounds. *Cell Biol. Int.* **1997,** *21*(10), 619–633.
6. Colliver, T. L.; Brummel, C. L.; Pacholski, M. L.; Swanek, F. D.; Ewing, A. G.; Winograd, N. Atomic and Molecular Imaging at the Single-Cell Level with TOF-SIMS. *Anal. Chem.* **1997,** *69*(13), 2225–2231.
7. Pacholski, M. L.; Cannon, D. M., Jr.; Ewing, A. G.; Winograd, N. Static Time-of-Flight Secondary Ion Mass Spectrometry Imaging of Freeze-Fractured, Frozen-Hydrated Biological Membranes. *Rapid Commun. Mass Spectrom.* **1998,** *12*(18), 1232–1235.
8. Gillen, G.; Roberson, S.; Ng, C.; Stranick, M. Elemental and Molecular Imaging of Human Hair Using Secondary Ion Mass Spectrometry. *Scanning* **1999,** *21*(3), 173–181.
9. McCandlish, C. A.; McMahon, J. M.; Todd, P. J. Secondary Ion Images of the Rodent Brain. *J. Am. Soc. Mass Spectrom.* **2000,** *11*(3), 191–199.
10. Chandra, S.; Smith, D. R.; Morrison, G. H. Subcellular Imaging by Dynamic SIMS Ion Microscopy. *Anal. Chem.* **2000,** *72*(3), 104A–114A.
11. Lorey, D. R., II; Morrison, G. H.; Chandra, S. Dynamic Secondary Ion Mass Spectrometry Analysis of Boron from Boron Neutron Capture Therapy Drugs in Co-Cultures: Single-Cell Imaging of Two Different Cell Types Within the Same Ion Microscopy Field of Imaging. *Anal. Chem.* **2001,** *73*(16), 3947–3953.
12. Todd, P. J.; Schaaff, T. G.; Chaurand, P.; Caprioli, R. M. Organic Ion Imaging of Biological Tissue with Secondary Ion Mass Spectrometry and Matrix-Assisted Laser Desorption/Ionization. *J. Mass Spectrom.* **2001,** *36*(4), 355–369.
13. Slodzian, G.; Daigne, B.; Girard, F.; Boust, F.; Hillion, F. Scanning Secondary Ion Analytical Microscopy with Parallel Detection. *Biol. Cell* **1992,** *74*(1), 43–50.
14. Peteranderl, R.; Lechene, C. Measure of Carbon and Nitrogen Stable Isotope Ratios in Cultured Cells. *J. Am. Soc. Mass Spectrom.* **2004,** *15*(4), 478–485.
15. Lechene, C.; Cotanche, D.; Benson, D.; Bonventre, J.; Distel, D.; Hillion, F.; Hentschel, D.; Kampf, J. P.; Kleinfeld, A. M.; Luyten, Y.; Schwartz, M.; Slodzian, G. High resolution quantitative imaging of biological cells using stable isotope mass spectrometry, submitted for publication.
16. Abumrad, N.; Harmon, C.; Ibrahimi, A. Membrane Transport of Long-Chain Fatty Acids: Evidence for a Facilitated Process. *J. Lipid Res.* **1998,** *39*(12), 2309–2318.
17. Berk, P. D.; Stump, D. Mechanisms of Cellular Uptake of Long Chain Free Fatty Acids. *Mol. Cell Biochem.* **1999,** *192*, 17–31.
18. Hamilton, J. A. Fatty Acid Transport: Difficult or Easy? *J. Lipid Res.* **1998,** *39*(3), 467–481.
19. Hamilton, J. A.; Johnson, R. A.; Corkey, B.; Kamp, F. Fatty Acid Transport: The Diffusion Mechanism in Model and Biological Membranes. *J. Mol. Neurosci.* **2001,** *16*(2/3), 99–108; Discussion 151–157.
20. Kleinfeld, A. M. Lipid Phase Fatty Acid Flip-Flop, is it Fast Enough for Cellular Transport? *J. Membr. Biol.* **2000,** *175*(2), 79–86.

21. Zakim, D. Thermodynamics of Fatty Acid Transfer. *J. Membr. Biol.* **2000,** *176*(2), 101–109.
22. Schwieterman, W.; Sorrentino, D.; Potter, B. J.; Rand, J.; Kiang, C. L.; Stump, D.; Berk, P. D. Uptake of Oleate by Isolated Rat Adipocytes is Mediated by a 40-kDa Plasma Membrane Fatty Acid Binding Protein Closely Related to that in Liver and Gut. *Proc. Natl. Acad. Sci. U.S.A.* **1988,** *85*(2), 359–563.
23. Abumrad, N. A.; el-Maghrabi, M. R.; Amri, E. Z.; Lopez, E.; Grimaldi, P. A. Cloning of a Rat Adipocyte Membrane Protein Implicated in Binding or Transport of Long-Chain Fatty Acids that is Induced During Preadipocyte Differentiation. Homology with Human CD36. *J. Biol. Chem.* **1993,** *268*(24), 17665–17668.
24. Kumar, G. B.; Black, P. N. Bacterial Long-Chain Fatty Acid Transport. Identification of Amino Acid Residues Within the Outer Membrane Protein FadL Required for Activity. *J. Biol. Chem.* **1993,** *268*(21), 15469–15476.
25. Schaffer, J. E.; Lodish, H. F. Expression Cloning and Characterization of a Novel Adipocyte Long Chain Fatty Acid Transport Protein. *Cell* **1994,** *79*(3), 427–436.
26. Civelek, V. N.; Hamilton, J. A.; Tornheim, K.; Kelly, K. L.; Corkey, B. E. Intracellular pH in Adipocytes: Effects of Free Fatty Acid Diffusion Across the Plasma Membrane, Lipolytic Agonists, and Insulin. *Proc. Natl. Acad. Sci. U.S.A.* **1996,** *93*(19), 10139–0144.
27. Cooper, R. B.; Noy, N.; Zakim, D. Mechanism for Binding of Fatty Acids to Hepatocyte Plasma Membranes. *J. Lipid Res.* **1989,** *30*(11), 1719–1726.
28. Hamilton, J. A.; Civelek, V. N.; Kamp, F.; Tornheim, K.; Corkey, B. E. Changes in Internal pH Caused by Movement of Fatty Acids Into and Out of Clonal Pancreatic β-Cells (HIT). *J. Biol. Chem.* **1994,** *269*(33), 20852–20856.
29. Kamp, F.; Zakim, D.; Zhang, F.; Noy, N.; Hamilton, J. A. Fatty Acid Flip-Flop in Phospholipid Bilayers is Extremely Fast. *Biochemistry* **1995,** *34*(37), 11928–11937.
30. Srivastava, A.; Singh, S.; Krishnamoorthy, G. Rapid Transport of Protons Across Membranes by Aliphatic Amines and Acids. *J. Phys. Chem.* **1995,** *99*, 11302–11305.
31. Cupp, D.; Kampf, J. P.; Kleinfeld, A. M. Fatty Acid-Albumin Complexes and the Determination of the Transport of Long Chain Free Fatty Acids Across Membranes. *Biochemistry* **2004,** *43*(15), 4473–4481.
32. Kampf, J. P.; Kleinfeld, A. M. Fatty Acid Transport in Adipocytes Monitored by Imaging Intracellular FFA Levels. *J. Biol. Chem.* **2004,** *279*, in press.
33. Hallegot, P.; Peteranderl, R.; Lechene, C. In-Situ Imaging Mass Spectrometry Analysis of Melanin Granules in the Human Hair Shaft. *J. Invest. Dermatol.* **2004,** *122*(2), 381–386.
34. Green, H.; Kehinde, O. Spontaneous Heritable Changes Leading to Increased Adipose Conversion in 3T3 Cells. *Cell* **1976,** *7*(1), 105–113.
35. Richieri, G. V.; Ogata, R. T.; Kleinfeld, A. M. A Fluorescently Labeled Intestinal Fatty Acid Binding Protein. Interactions with Fatty Acids and Its Use in Monitoring Free Fatty Acids. *J. Biol. Chem.* **1992,** *267*(33), 23495–23501.
36. Anel, A.; Richieri, G. V.; Kleinfeld, A. M. Membrane Partition of Fatty Acids and Inhibition of T Cell Function. *Biochemistry* **1993,** *32*(2), 530–536.
37. Kamp, F.; Guo, W.; Souto, R.; Pilch, P. F.; Corkey, B. E.; Hamilton, J. A. Rapid Flip-Flop of Oleic Acid Across the Plasma Membrane of Adipocytes. *J. Biol. Chem.* **2003,** *278*(10), 7988–7995.
38. Peitzsch, R. M.; McLaughlin, S. Binding of Acylated Peptides and Fatty Acids to Phospholipid Vesicles: Pertinence to Myristoylated Proteins. *Biochemistry* **1993,** *32*(39), 10436–10443.